MAX-PLANCK-INSTITUT FÜR PLASMAPHYSIK

GARCHING BEI MÜNCHEN

An Improved Retarding Field Analyser

P. Staib

IPP 9/5 Februar 1972

Die nachstehende Arbeit wurde im Rahmen des Vertrages zwischen dem Max-Planck-Institut für Plasmaphysik und der Europäischen Atomgemeinschaft über die Zusammenarbeit auf dem Gebiete der Plasmaphysik durchgeführt.

Februar 1972

Abstract

A new electrostatic energy analyser is presented. It uses two sets of spherical grids. The first one is a retarding field arrangement in which the particles are decelerated down to energies close to zero. The transmission properties of the retarding field are presented. The particles enter the second part, an inverted spherical accelerating set which sharply focusses the low energy particles into the entrance aperture of a multiplier, whereas the high energy part misses the aperture. By cutting out the fast part, only a narrow energy band reaches the detector and a high signal-to-noise ratio results.

Introduction

High sensitivity analyses of secondary electron energies, i. e. the detection of meaningful signals above the noise level, remains an important problem in surface effects measurements such as for Auger or photoelectron spectroscopy. High sensitivity analysers have been designed to attempt the best compromise between intensity, resolving power and signal-to-noise ratio. The cylindrical mirror analyser is an example and is widely used for secondary electron spectroscopy (BLAUTH 1957, GERLACH 1971, PALMBERG 1969, ZASHKVARA 1970). A compromise based on the spherical retarding field analyser was proposed for photoelectron spectroscopy (ESCA) (HUCHITAL 1970).

The arrangement we present here provides a great improvement of the characteristics of a spherical retarding field analyser. By adjoining a focussing part it is possible to increase the signal-to-noise ratio and to use an electron multiplier as detector.

1. Description of the energy analyser

The analyser is shown in Fig. 1 and consists of two spherical parts A and B which are sets of two spherical concentric grids (like those provided for LEED assembly). The source is located at the centre of the set A, which is used as the spherical retarding field part by applying a suitable potential U_A between the two grids. Particles with a charge e emitted by the source must lose an amount eU_A of kinetic energy passing through the set. If not reflected, they appear in the space behind A with a kinetic energy ε . This space between the sets A and B is electrically closed by the cylindrical grid C, which is set at a potential slightly higher than the common potential of grids A2 and B1 in order to repel the particles having the lowest energies ε . An accelerating voltage U_B is applied between the grids of set B. Particles reaching this set undergo radial acceleration and gain a kinetic energy of eU_B. The entrance aperture D of a detector system is located at (or near) the common centre of the grids B. Those particles having an energy $\varepsilon \ll eU_B$ will have a fairly radial trajectory and pass through the aperture D. The others with higher ε values miss it and are not detected: in contrast with the arrangement of HUCHITAL, only a narrow energy line is registered. The focussing set B is not used to collect all the retarted particles as with SAMSON (1968), but performs true energy selection.

2. The retarding field part A

A spherical retarding field allows a large entrance solid angle together with a relatively large source area, and so the intensity of the analysed particle flux is large (HUCHITAL 1970, HEDDLE 1971). In the energy range in which the retarding field exerts energy selection on the particle flow, the transmission function of the grid A2 depends on geometrical factors such as the area of the source, radius of the grid, and one electrical factor, the product F.a, F being the electric field strength in the retarding region and a being the wire spacing of the grid.

The shape of the transmission function was determined by computing the trajectories of a particle beam normally incident to the grid surface. We chose a periodic potential closely approximating the electrostatic field of the retarding grid and counted how many particles of the beam would overcome the potential wall and be transmitted (STAIB 1972). No field was applied behind the retarding grid A2. The transmission function $T(\varepsilon)$ is obtained by varying the kinetic energy of the incident beam. An important feature of this result is the strong increase of the transmission values at the threshold energy: 50 % transmission is obtained for an energy shift from the threshold of

$$\varepsilon_{0.5} \backsimeq 5.10^{-2} \, . \quad F.a$$

where ε is the energy in eV, F the electrical field strength in the retarding space in V/m, and a the distance of the mesh wires in m.

For a field strength of one volt per length a, the 50 % value is reached for $\varepsilon = 50$ meV. This value is lower than expected on the simple assumption that the resolving power is given by the potential difference between the grid wires and the centre of the holes (HEDDLE 1971)

$$\Delta v \backsimeq F.a/2\pi = 16.10^{-2} \; F.a$$

Curve A of fig. 4 shows the shape of the transmission function $T(\varepsilon)$ for an experimental field strength of 15 V per distance a.

3. The focussing part B

This part allows the selection of particles with the lowest kinetic energies, i.e. smaller than a few eV in our case. With the notation of fig. 2, the incoming particle with the kinetic energy ε reaches the grid of radius R at an incidence angle ψ. The energy can be split into two components, a radial $\varepsilon_R = \varepsilon \cos^2 \psi$ and a transverse $\varepsilon_T = \varepsilon \sin^2 \psi$ one, corresponding to the radial and transverse components of the velocity. When the particles pass through the set, the radial energy increases by eU_B, while the transverse energy is conserved. If the distance between the grids is small in comparison with its radius B, the set is equivalent to a spherical surface separating the medium of refractive index n = 1 (space between set A and B) and $n(\varepsilon) = (1+eU_B/\varepsilon)^{1/2}$ (space of the detector system). The detector aperture exerts energy selection on the refracted flow. The detected intensity distribution $I(\varepsilon)$ for a point source is the result of, firstly, the spherical aberation of the focussing part and, secondly, the diameter ϕ of the detector aperture. The spherical aberration would be reduced by using grid surfaces generated by the rotation of a Cartesian oval, thus causing a stigmatic focussing of the source on the rotation axis. We computed the distribution $I(\varepsilon)$ of particles emitted from a point source and escaping with an isotropic velocity distribution.

We first neglect the scattering effects of the grids. The particles overcoming the retarding field seem to originate from the source with an energy ε and are refracted. Applying the refraction law at one point of the grid surface, we can evaluate the energy of particles impinging on the grid at this point and passing through the detector aperture. Integration over the grid surface gives the measured intensity distribution $I(\varepsilon)$. Results of numerical integration are given in fig. 3 for some positions of the aperture on the symetric axis. The reduced energy parameter is $\eta = \varepsilon/eU_B$ and the values of the geometrical data are listed in fig. 2. The distribution shows a threshold at lower energies corresponding to the first detected particle refracted at the outer range of the grids. By increasing the energy ε, more and more area of the grids "illuminates" the aperture up to a maximum for which the whole surface focusses the particles through the aperture. A further increase of ε reduces the active surface and the intensity decreases. The screen S in fig. 1, centred on the rotation axis of the system, cuts off detection at high energies.

The above calculation is based on the assumption that the particles are not scattered before they reach the set B. This is not true of the lowest values of the kinetic energy ε, for which scattering effects in the potential of the retarding grid become important (STAIB 1972). Further the cylindrical grid C will increase these effects. Let us now assume that the scattering is very large and leads to an isotropic velocity distribution into the space between the sets A and B. Even in this case good energy selection is possible if the aperture is located at the centre of the grids. The incidence angle ψ is no longer definite and varies from zero to $\pi/2$. As a consequence of the high value of the refraction index n at low values of ε, all particles are refracted into a cone with an aperture angle α given by

$$\sin \alpha = n^{-1} = (1+eU_B/\varepsilon)^{-1/2}$$

We get the intensity distribution by calculating the solid angle $\Omega(\varepsilon)$ containing the velocity of incident particles being detected and integrated over the surface of the grid. The result is depicted by the dashed curve in fig. 3. The distribution shows a maximum for η near zero corresponding to the case that all particles with the energy ε are detected. With increasing η, the refracted beam becomes broader and the intensity decreases. There is no cut off for high energies in this case.

4. Resolving power

The resolving power of the analyser is obtained by considering separately the contributions of the retarding and focussing parts. The resolution of the retarding field can be expressed by:

$$\Delta U_A = e \sqrt{(5.10^{-2} F.a)^2 + (\tfrac{s}{R_1})_1^4 U_A^2}$$

The first contribution is provided by the 50 % transmission value of the retarding grid and the second is a simple way of taking into account the energy broadening due to the source radius s (R_1 is the radius of the first grid A_1). To obtain a higher resolution, it is necessary to make the product F.a small, that is to choose a dense mesh and a large distance between the grids.

The resolution of the focussing part is determined by the ratio ϱ/R between the radius of the detector aperture and the mean radius of the focussing grid, and by the value of the focussing voltage V_B. In the case d = o, the resolution is very roughly given by:

$$E_B \backsim 3 \cdot (\frac{\varrho}{R})^2 eV_B$$

This theoretical value is small and can only be reached by using perfectly spherical grids (deviation from the ideal sphere lower than ϱ) and ensuring exact compensation of the earth's magnetic field.

5. Experimental results

The simplest way to build the analyser is to use the grids of a LEED assembly. The radii are 55.5, 58.1, 60.7 and 63.4 mm in our case. A Channeltron multiplier is used as detector together with an aperture D with a 2 mm diameter. Other experimental values are listed in fig. 2. No shielding of the earth s magnetic field is provided. A broad angular distribution of electron velocities is obtained by elastic scattering of a monoenergetic electron beam from a metallic sample. The experimental shape of an energy line is shown in fig. 4 for a primary electron energy of 150 eV and a focussing potential of 100 eV. The resolving power is defined as

$$A = (\Delta E - \Delta E_o) / E$$

with ΔE being the full width at half maximum of the line of energy E, ΔE_o being the full width for energies extrapolated to zero. The value of A is quite constant over the energy range 50 to 500 eV and is A = 0.8 %. The value $\Delta E_o = 1.4$ eV was found by extrapolation. The main limitation of the resolving power is due to the poor sphericity of the grids.

An important feature of the analyser is that the resolving power can be set without any mechanical change by a suitable choice of the focussing voltage U_B and the repelling potential of grid C. Examples are shown in fig. 5 : curves (A) show that with increasing U_B the intensity rises and the high energy side of the line is enlarged; curves (B) show for increasing repelling potential higher intensities and enlarged low energy side because of the presence of a variable electric field behind the grid A 2.

6. Conclusion

An exact calculation of the optical properties of the analyser is very difficult because of the multiple scattering suffered by the particles. It is possible, however, to get a fair description of the properties, lying between two extremal assumptions of no scattering and maximum scattering effects.

Comparing the analyser with a classical 4-grid retarding field optical system, the gain in sensitivity is remarkable. For the same entrance solid angle of about π steradian, firstly the analyser gives an energy line instead of an energy step in the measured intensity distribution and secondly the focussing allows the use of an electron multiplier.

Looking at its performance, resolving power of 0.8 % and FWHM of 5.4 eV at E = 500 eV, the new analyser may be compared with a cylindrical mirror analyser described by PALMBERG et al. (1969) having similar dimensions and resolving power. Applying the criterion given by SAR EL (1970) we evaluate the luminosity L = T.S as the product of the point source transmission value T and the area of the entrance slits or source surface in this case. We prefer this criterion to that proposed by HUCHITAL (1970) or HEDDLE (1971) based on the étendue value, i.e. the product of the entrance area and entrance solid angle. The étendue measures the intensity entering the analyser where as the luminosity, involving the transmission value, measures the output intensity. In our case, the transmission T is the product of the entrance solid angle, about π steradian, and the optical transmission of the four grids $(0.75)^4 = 0.32$. This ist 16 % of the maximum value $T = 2\pi$. The source area S is much larger for a retarding field than in other dispersive devices because the resolving power is a square function of the source diameter instead of a linear function of the dispersive analyser. The diameter of the source area was 2 mm and the luminosity is

$L = \pi (0.16) = 0.5\ mm^2$. For the cylindrical mirror analyser of PALMBERG (1969) the source diameter was 0.1 mm and the transmission value 10 %, giving a luminosity $L = \pi (0.05)^2 (0.1) = 8.10^{-4}\ mm^2$. This comparison shows that the new analyser would be preferable in cases where particles from a large source area are to be analysed e.g. in photoelectron spectroscopy.

Acknowledgement

The author is grateful to H. Liebl for his critical reading of the manuscript and to H. Heil for stimulating discussions.

Appendix I

Computation of the intensity distribution $I(\eta)$ without scattering effects.

We assume that the particles escape the point source with an isotropic velocity distribution. We have to calculate the following integral:

$$I(\eta) = \int_{\theta_{o\,min}}^{max} dI(\theta_o) = \sum_{i=1}^{1500} \delta I(\theta_{o,i}) . T$$

There fore, we decompose the integration into 1500 steps for θ_o (fig. AI) that is we devide the spherical surface into the same amount of thin rings having an area $d\sigma = 2\pi \sin\theta\ d\theta$. If the refracted beam passing through the detector aperture is T = 1 and the intensity contribution is $dI = I_o \cdot 2\pi \sin\theta_o \cdot d\theta_o$ where I_o is the flux of particle emitted by the source in 1 sr. If the beam misses the aperture is T = o and there is no contribution dI. The sum of the dI gives the intensity I for a value of η . The flow-chart diagram is given below and the following expressions are used:

1. $n = (1+1/\eta)^{1/2}$
2. $\psi = \arcsin(D/R \sin\theta_o)$
3. $\theta = \psi - \theta_o$
4. $r = \arcsin(\sin\psi/n)$
5. $r_1 = \text{arctg}\left[R\cos\theta + D/(R\sin\theta - p) \right] + \theta - \pi/2$
   $r_2 = \text{arctg}\left[R\cos\theta + D/(R\sin\theta + p) \right] + 0 - \pi/2$
6. $dI = \sin\theta_o / 62.834$

Appendix II

Computation of the intensity distribution $I(\eta)$ with maximal scattering effects.

We assume now that the particle flow suffers large scattering effects before they reach the focussing set. The incidence angle varies between 0 and $\pi/2$ and we assume the velocity distribution to be isotropic. We consider only the case d = o with the detector aperture located at the centre of the set. We divide the surface into 100 thin rings giving each an intensity contribution

$$dI = 2\pi R \sin\theta \cdot \frac{\Omega}{2\pi} \cdot d\theta$$

The solid angle includes all the particle being transmitted and is evaluated from $\psi(\xi)$ i.e. from $r(\xi)$ through the refraction law. The flow-chart diagram is given below and the following expressions are used:

1. $n = (1+1/\eta)^{1/2}$
2. $r = \text{arctg}\left[0.02 (1-\cos^2\psi\cos\theta)^{1/2} \right]$
3. $\psi = \arcsin(n \sin r)$
4. $\Omega = \int_{\xi=o}^{2\pi} (1 - \cos\psi)\, d\xi$
5. $dI = \Omega \sin\theta\ d\theta$

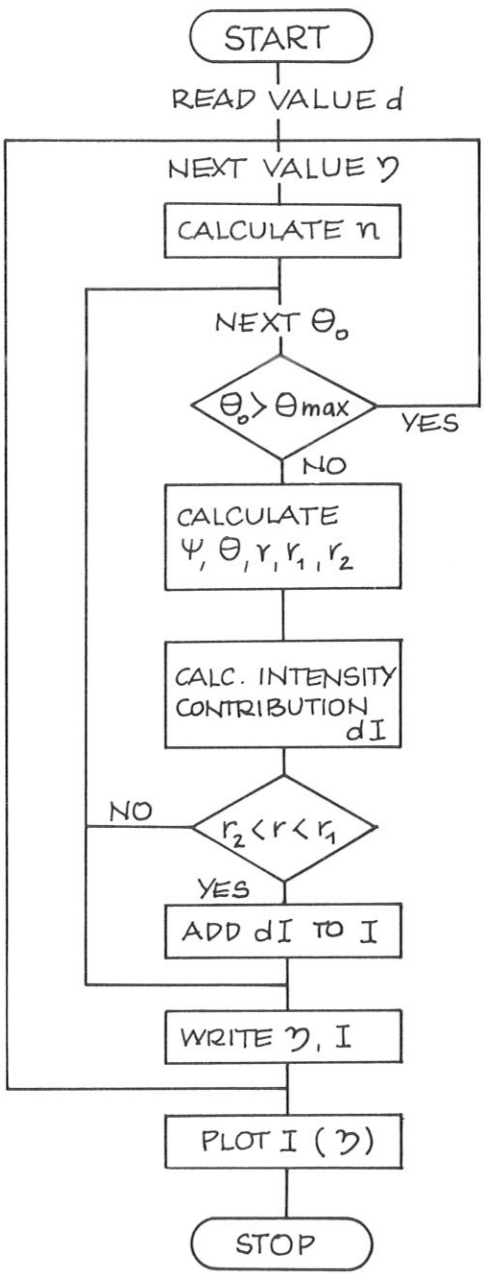

FLOWCHART A I

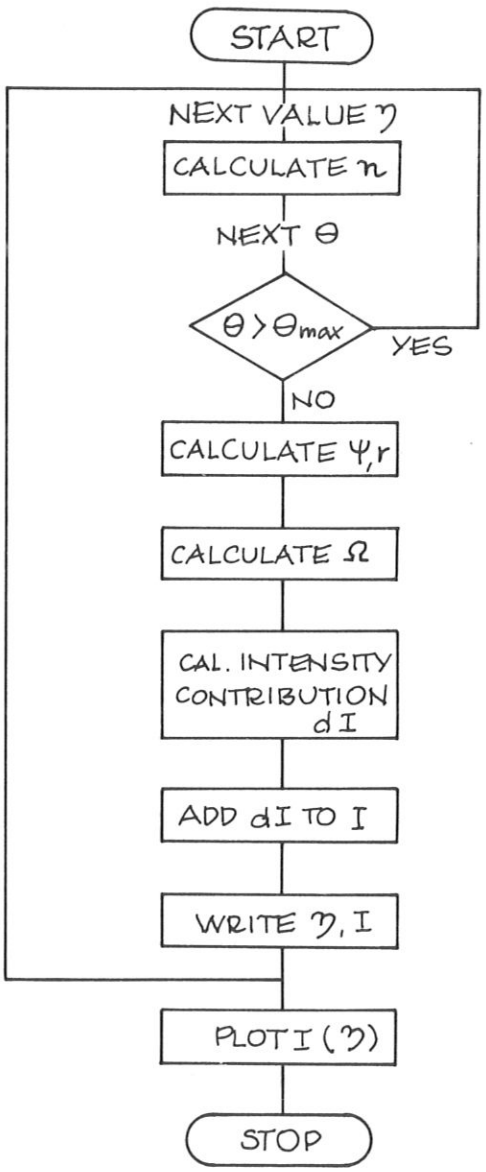

FLOWCHART A II

References

BLAUTH, E.W. (1957), Z. Phys. 147 , 228-40

GERLACH, R.L. (1971), J. Vac. Sci. and Tech. 8 , 599 - 604

HEDDLE, D.W.O. (1971), J. of Physics E: Sci. Intr. 4 , 589-92

HUCHITAL, D.A. and RIGDEM J.D. (1970), Appl. Phys. Letters, 16 , 348-51

PALMBERG, P.W., BOHN, G.K. and TRACY I.C. (1969), Appl. Phys. Letters 15 , 254-5

SAMSON, J.A.R. and CAIRNS R.B. (1968), Phys. Rev. 173 , 80-85

SAR-EL,H.Z. (1970), Rev. Sci. Instr. 41 , 561-4

STAIB, P. (1972), IPP-Report, under preparation

ZASHKVARA, V.V., KORSUNSKIIMI, RED KIN V.S. and LAVROV V.P. (1971), Soviet Phys.-Techn. Phys. 15 , 2033-4

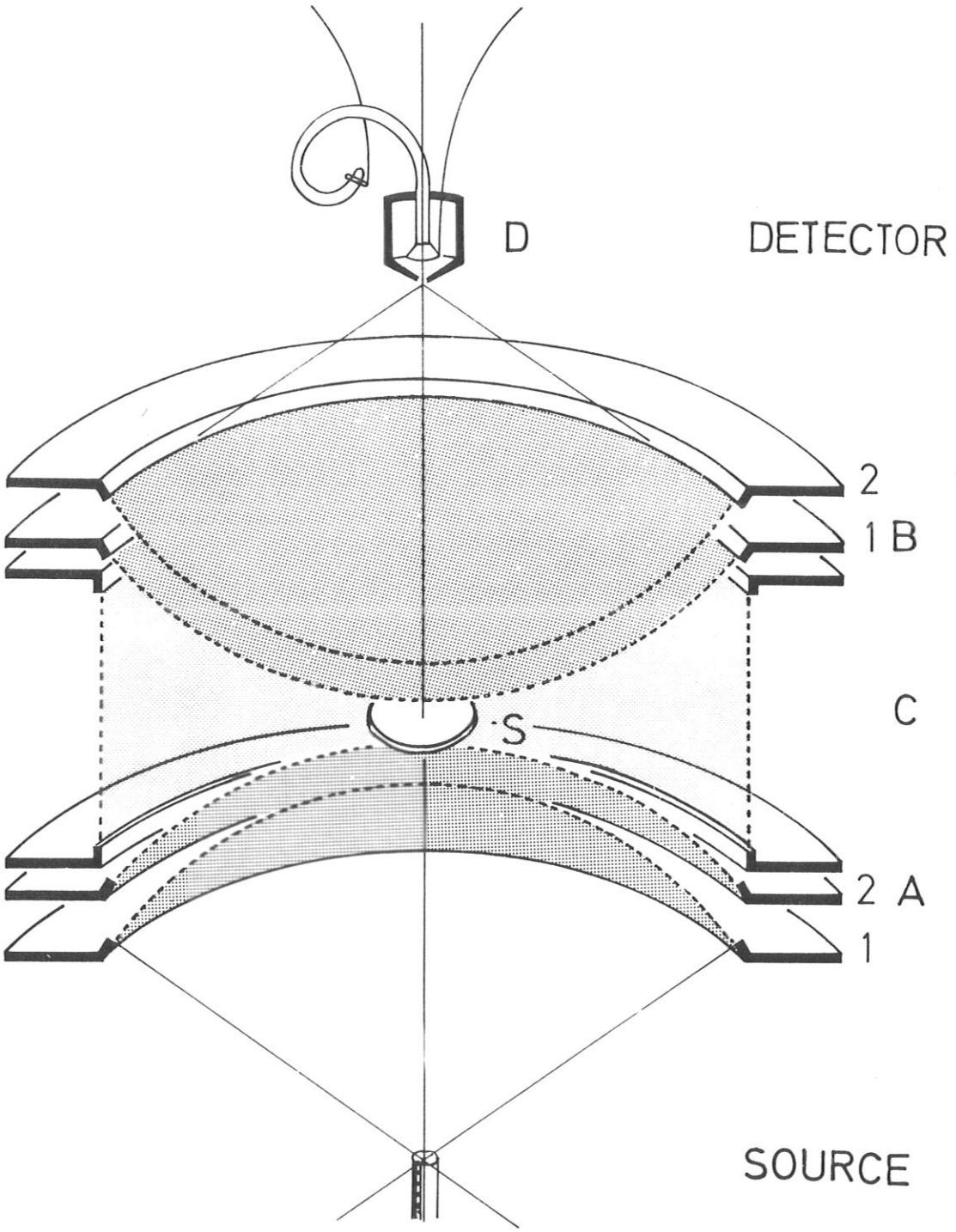

Fig. 1 View of the energy analyser showing the two sets A and B of spherical concentric grids, the cylindrical grid C and the screen S.

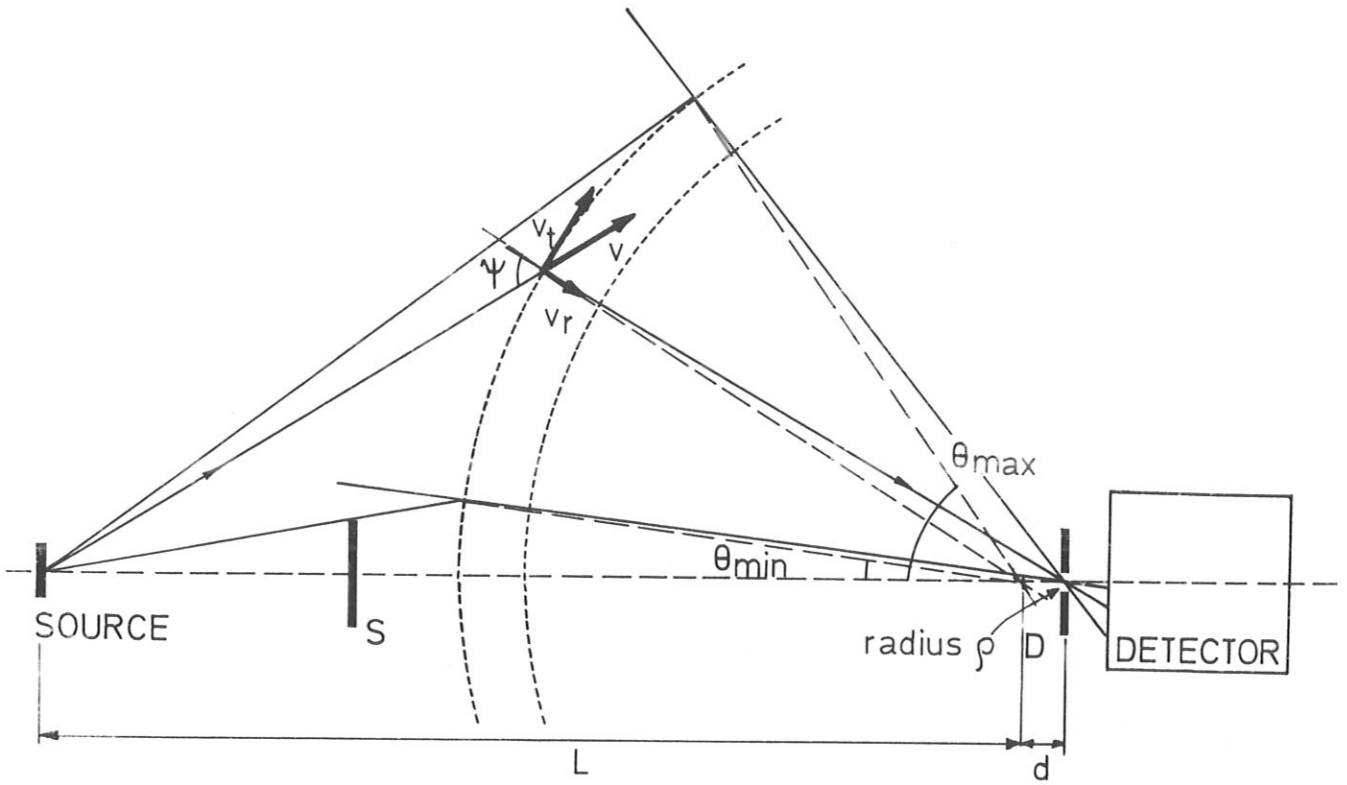

Fig. 2 Geometrical parameters of the focussing part:

R = 1 Mean radius of the grids. Distance between grids assumed to be much lower than R.

L = 2.5 Distance from the source to the centre of the grid.

d = Variable distance between the detector aperture D and the centre of the grids.

θ_{min} = 0.1 radian and θ_{max} = 1.0 radian are the angles that limit the active surface of the grids.

ρ = 0.02 Radius of the aperture D.

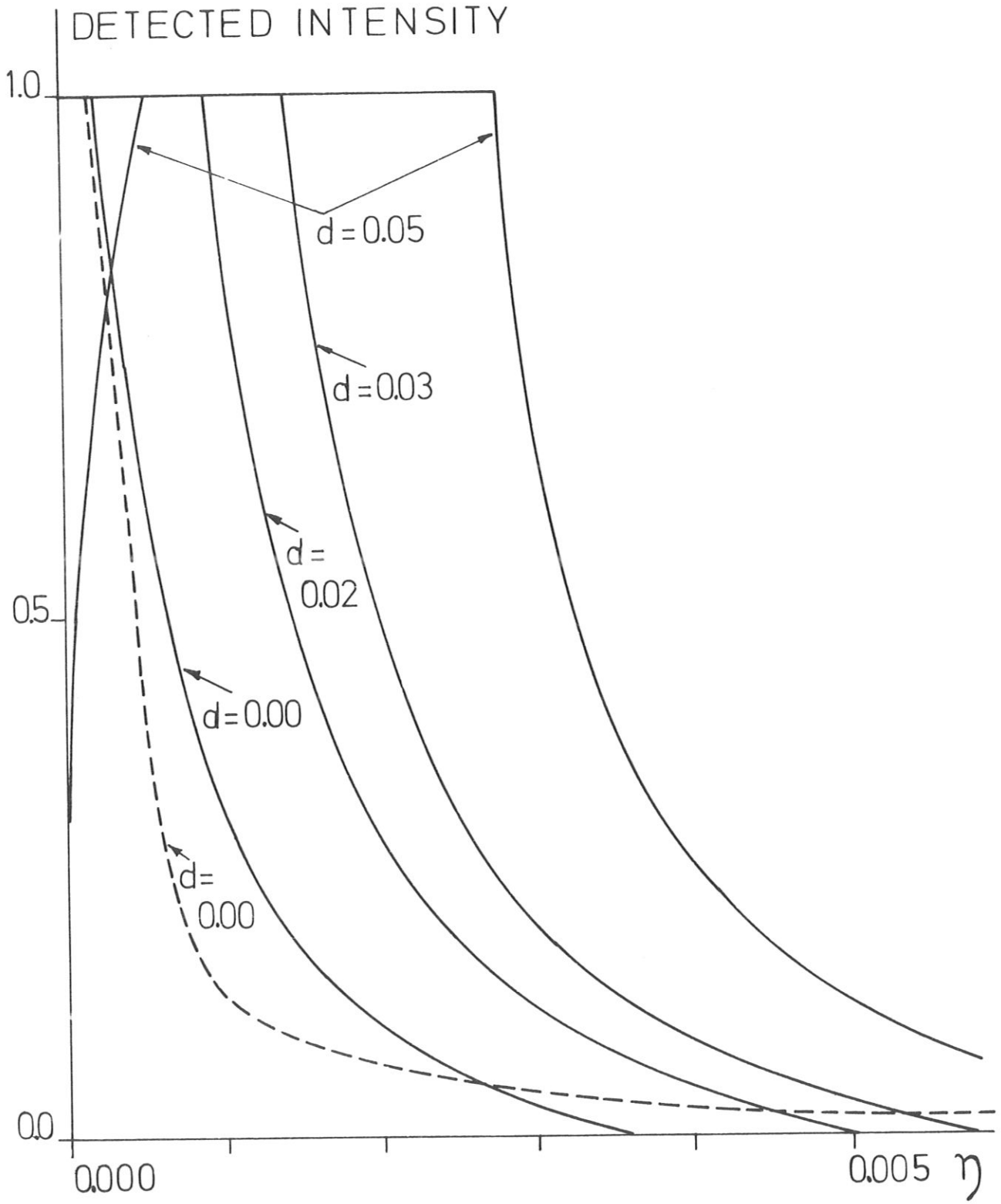

Fig. 3 Full lines = calculated intensity distribution for source positions of D, scattering effects neglected.
Dashed lines = calculated intensity distribution for the aperture located at the centre of the grids (d = o) and for maximum scattering effects.
The reduced energy parameter is $\eta = \varepsilon / eU_B$.

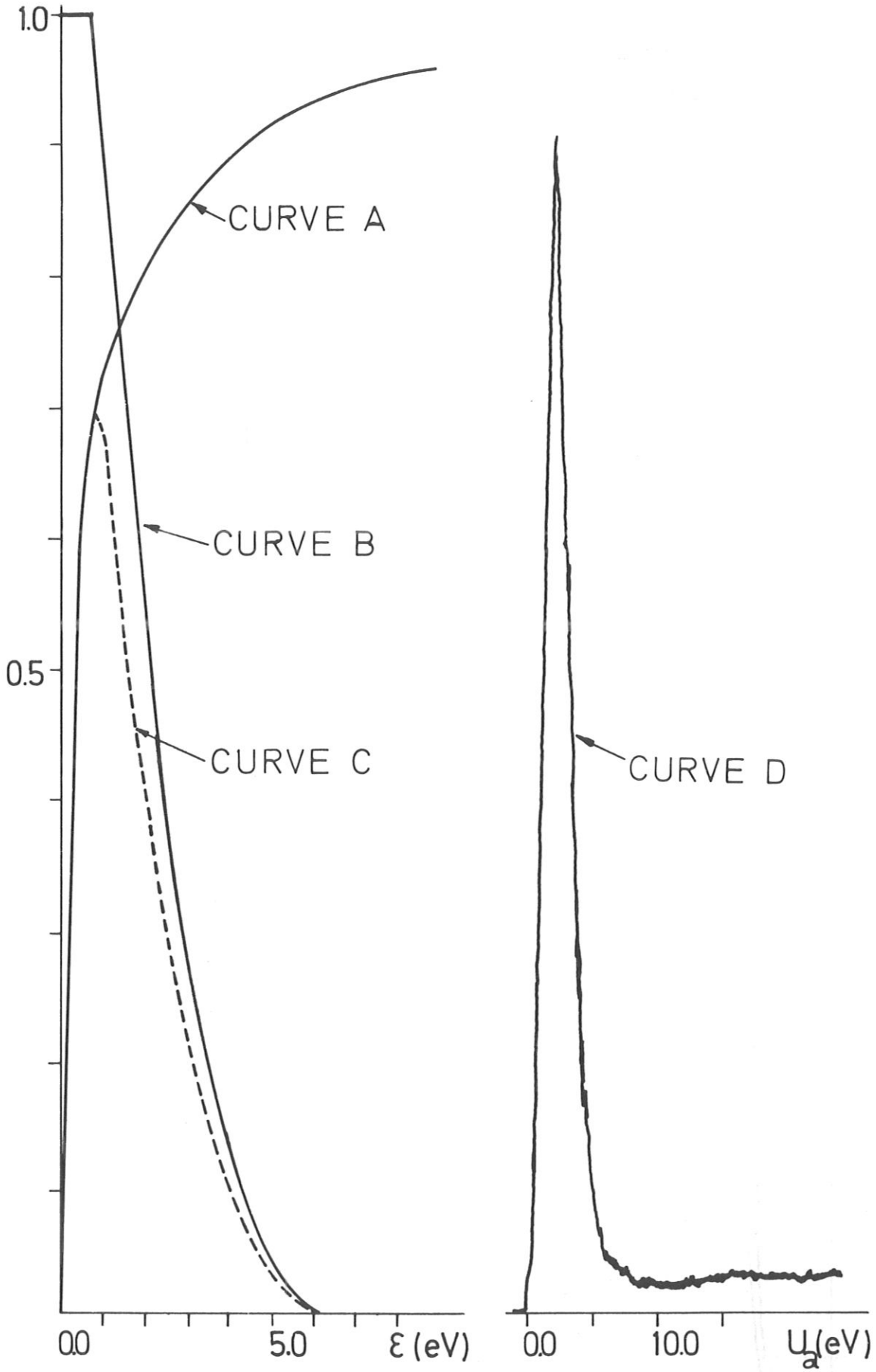

Fig. 4 Curve A = computated transmission function of the retarding part A for a field strength of 8 V per distance between the mesh wires.

Curve B = transmission function of the focussing part B for d = 0.03 and U_B = 100 V.

Curve C = shape of the resulting intensity distribution.

Curve D = typical experimental line shape for a primary energy of 150 eV and a focussing voltage U_B = 100 V.

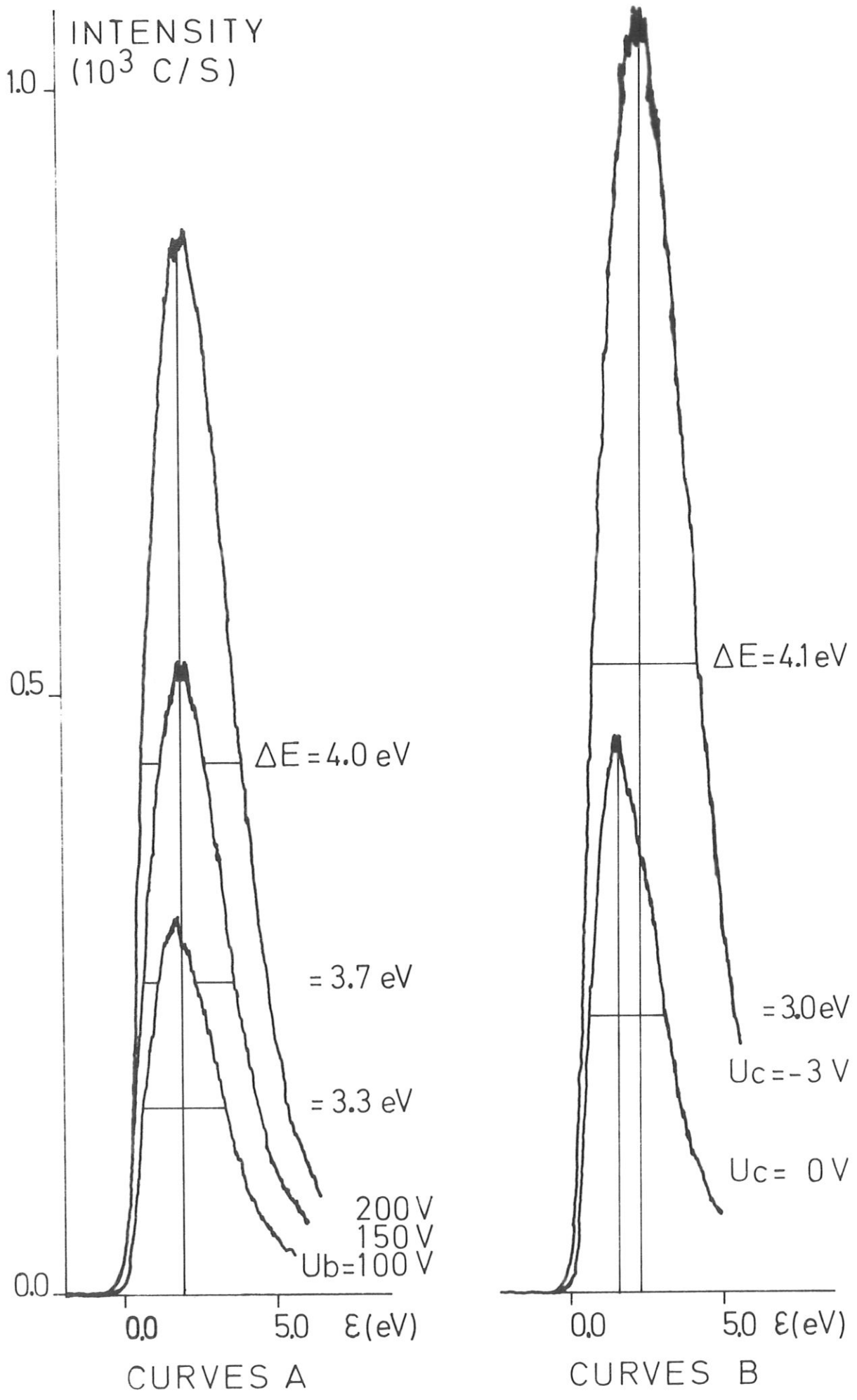

Fig. 5 Electrical setting of the intensity and resolving power (See text).

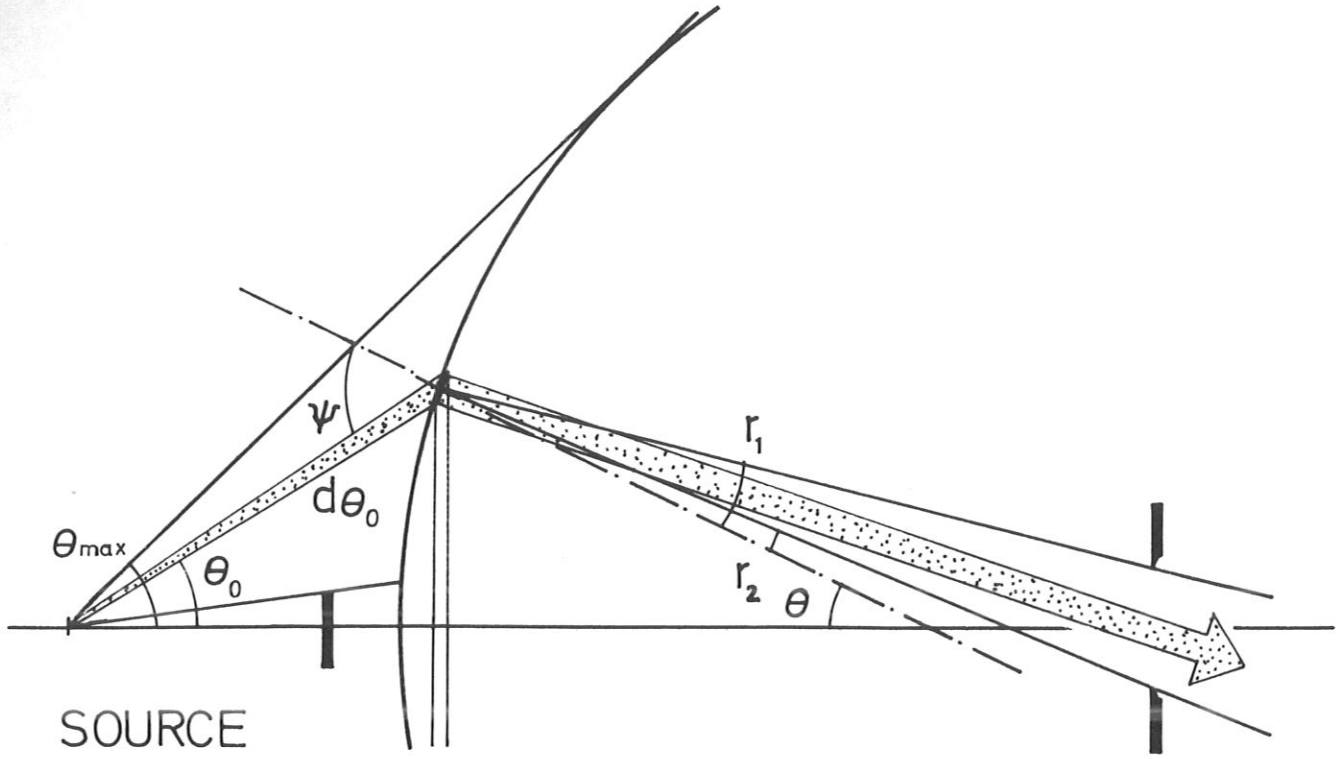

fig. AI

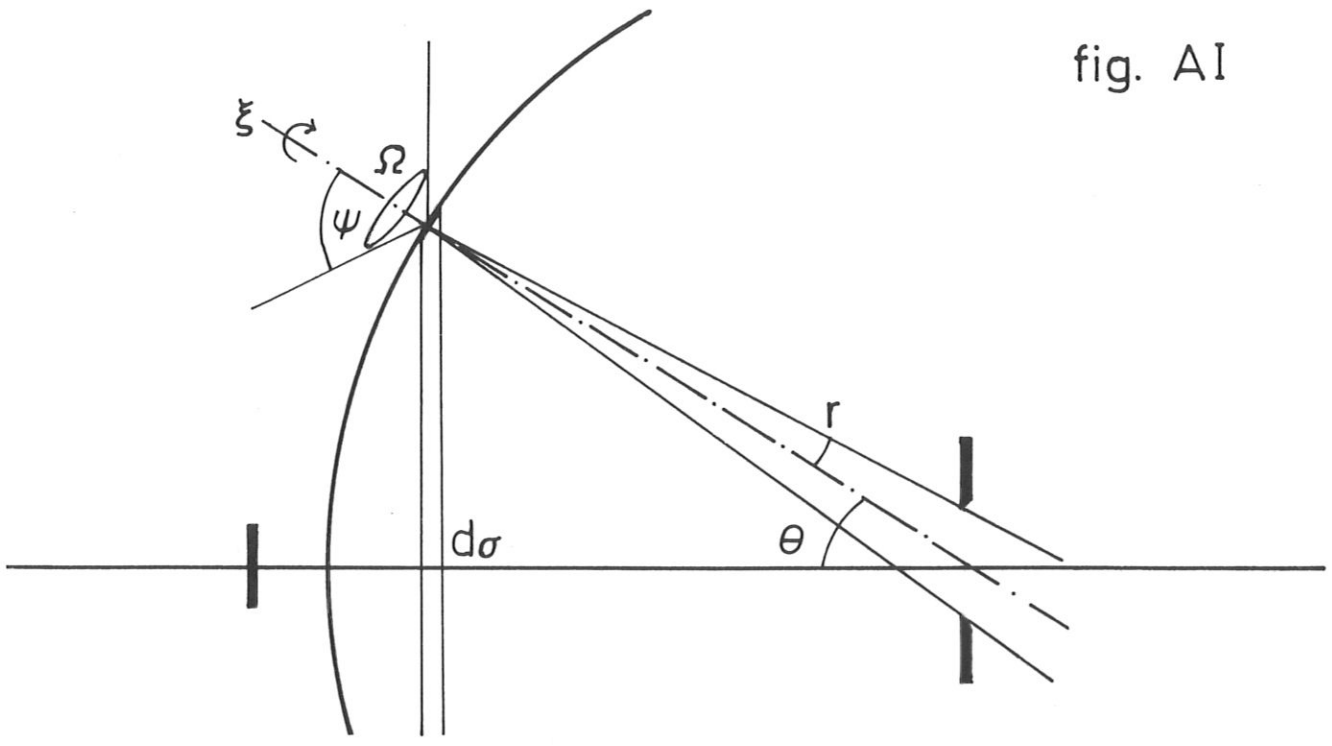

fig. AII